

This is the peer reviewed version of the following article:

Pulsed current hard anodizing of heat treated aluminum alloys: Frequency and current amplitude influence / Bononi, Massimiliano; Giovanardi, Roberto; Bozza, Andrea. - In: SURFACE & COATINGS TECHNOLOGY. - ISSN 0257-8972. - 307:(2016), pp. 861-870. [10.1016/j.surfcoat.2016.10.025]

Terms of use:

The terms and conditions for the reuse of this version of the manuscript are specified in the publishing policy. For all terms of use and more information see the publisher's website.

19/12/2025 04:20

Accepted Manuscript

Pulsed current hard anodizing of heat treated aluminum alloys: Frequency and current amplitude influence

Massimiliano Bononi, Roberto Giovanardi, Andrea Bozza

PII: S0257-8972(16)31019-2
DOI: doi: [10.1016/j.surfcoat.2016.10.025](https://doi.org/10.1016/j.surfcoat.2016.10.025)
Reference: SCT 21670

To appear in: *Surface & Coatings Technology*

Received date: 26 July 2016
Revised date: 29 September 2016
Accepted date: 9 October 2016



Please cite this article as: Massimiliano Bononi, Roberto Giovanardi, Andrea Bozza, Pulsed current hard anodizing of heat treated aluminum alloys: Frequency and current amplitude influence, *Surface & Coatings Technology* (2016), doi: [10.1016/j.surfcoat.2016.10.025](https://doi.org/10.1016/j.surfcoat.2016.10.025)

This is a PDF file of an unedited manuscript that has been accepted for publication. As a service to our customers we are providing this early version of the manuscript. The manuscript will undergo copyediting, typesetting, and review of the resulting proof before it is published in its final form. Please note that during the production process errors may be discovered which could affect the content, and all legal disclaimers that apply to the journal pertain.

PULSED CURRENT HARD ANODIZING OF HEAT TREATED ALUMINIUM ALLOYS: FREQUENCY AND CURRENT AMPLITUDE INFLUENCE

*Massimiliano Bononi^a, Roberto Giovanardi^a, Andrea Bozza^b

^aUniversity of Modena and Reggio Emilia, Department of Engineering 'Enzo Ferrari', Via Vivarelli 10, 41125 Modena, ITALY.

^bMicrontech s.r.l., GPS-Mochem Group, Via A. Boito 431, Soliera, MO, Italy

ABSTRACT

Pulsed current hard anodizing procedures have been applied to the widely used heat treated aluminium alloys AA2024-T3, AA6082-T6 and AA7075-T6. The influence of frequency and of current amplitude on anodic oxide thickness, hardness, defectiveness, volumetric expansion ratio and on process faradic efficiency has been studied. Higher frequencies generate a decrease in coating electric resistance and in general they are less effective in order to overcome typical critical issues arising in alloys difficult to be anodized. In AA2024-T3 and AA6082-T6 higher frequencies led to slight increase in thickness, decrease in compactness and faradic efficiency while hardness remained almost constant or a bit higher. With higher frequencies in AA2024-T3 defective state significantly got worse, in AA6082-T6 it improved. In AA7075-T6 an almost frequency independent behaviour occurred. The highest wave amplitude with a slightly cathodic "off" current (reverse pulse) allowed to obtain greater thickness, hardness and compactness while other current amplitudes did not show significant influence on properties analyzed; a very low, but still anodic, "off" current however induced slight hardness decreases.

Keywords: hard anodizing, pulsed current, aluminium, intermetallic, electric, frequency

* Author to whom correspondence should be addressed, e-mail: massimiliano.bononi@unimore.it

1. INTRODUCTION

Anodizing is a widely used surface treatment in aluminum alloys which builds a protective coating increasing corrosion resistance and allowing post-processes with aesthetic purposes (decorative anodizing); the “hard” version further enhances abrasion resistance through a thick (up to $\sim 100\mu\text{m}$) and mechanical performing oxide almost always necessary in advanced structural applications (aerospace, military, motorsport, etc.) [1]. In these sectors, heat treatable aluminum alloys (series 2XXX, 6XXX and 7XXX) play a significant role thanks to their great high-mechanical-properties/low-density compromise [2].

Unfortunately alloying elements and precipitates, which contribute to age-hardening in heat treatable aluminium alloys [3], introduce on anodizing process critical issues making the obtainment of a hard, compact, low-defected and well-adherent oxide difficult [4]–[8]. The specific behavior of many different intermetallics during anodizing has been investigated; Mg_2Si , CuAl_2 , $\beta\text{-AlMg}$, Al-Zn-Mg particles were found to oxidize faster than Al-matrix while TiAl_3 , NiAl_3 and MnAl_6 at slower rate and FeAl_3 at similar rate [9], [10]. Another study stated that Al-Fe and Al-Fe-Si intermetallics tend to be occluded into anodic oxide while Al-Cu particles tend to be preferentially oxidized producing defected oxides [7]. Other works discovered that preferential oxidation of intermetallics depends upon anodization potential; Al-Cu-Mg particles oxidize faster also at low potentials while Al-Cu and Al-Cu-Fe intermetallics are inert at low potentials but they oxidize preferentially at high ones [11], [12]. Moreover, the higher the Cu content and the faster preferential oxidation of intermetallic occurs due to increase of oxygen evolution and associated cyclic disruption of the anodic oxide [4]. Fe and Mn impurities are also crucial in determining the quality of the anodic oxide; high amounts of those impurities present in Al-Fe-Mn-Si particles provoke steep voltage rise during treatment and a non-uniform growth of the anodic film [5], [13].

Summing up, the different phases present in the Al-matrix can introduce instabilities during anodizing treatment for the following reasons: i) different electric field distribution between

matrix and intermetallics so leading to an uneven anodic growth [1]; ii) entrapment of unoxidized metal particles into the anodic coating [1], [5], [13]–[18]; iii) oxygen evolution parasitic reaction typically caused by Al-Cu-Fe particles [4], [19], [20]. It's really important to find solutions to overcome these defects, not only to avoid low performing oxide and delamination, but also to limit the decrease in fatigue resistance intrinsically introduced by anodizing process [21]–[24].

In order to overcome these critical issues, some strategies try to modify the electrolytic solution [13], [25], [26], some others create on the component to be anodized a preliminary purer Al-based coating [21], [27], others vary the electric cycle applied. Within the latter, the fundamental common aim between the different approaches is to create precautionary conditions able to smooth inhomogeneities caused by the different properties between Al-matrix and second phases. Second phases induce different anodizing behavior in terms of anodic layer formation, ionic conductivity through the anodic layer and its dissolution. Moreover, the different electric conductivity between matrix and intermetallics induces electric field inhomogeneities that are responsible for the occurrence of temperature gradients due to the different joule effect phenomena and to the different oxide growth rate (oxidation is an exothermic reaction).

The employment of a pulsed current electric cycle is a solution which brings many advantages [28]–[30] including: i) electric double layer restoration; ii) heat dissipation; iii) barrier layer thinning (so reducing coating electric resistance); iv) a pause in oxide growth which enables the oxygen formed in parasitic reactions to be more easily removed out. These benefits, carried by time-off periods, are generally known and referred as “recovery effect” and are exploited on two fronts. From one side it is possible, mostly for easy anodizable alloys, to increase the mean current density applied so decreasing the process total duration [30], [31]; from the other side the smoothing properties of pulsed current are used for reducing defects

and critical issues on those alloys, such as casting alloys with high silicon content or heat treatable alloys, difficult to be correctly anodized [32]–[34].

As a result of a pulsed current modality, many variables are introduced on the system (current waveform, frequency, levels and times of current segments which make up the waveform). In literature, the study of those different variables is fragmented into different works which consider only some electric variables at one time, so it is actually difficult to understand their effective influence. Moreover different works, from which information could be assembled, often adopt different alloys or other process conditions (electrolyte, mean current, treatment duration, etc.) making data comparison and integration difficult.

Regarding current waveforms, Fratila-Apachitei et al. reported that this variable is not so crucial since no evident differences are found between different waveforms [32]; square-pulse one, characterized by “on” and “off” segments, is the most frequently adopted.

As regards frequency, two main approaches are found in literature: fast-pulse (frequency $> 10^1$ Hz [35]–[41]) and slow-pulse (frequency $< 10^{-1}$ Hz [30], [32]–[34], [42]). Studies on both techniques revealed improvements in anodic properties if compared to classic direct current anodizing. These two approaches were compared in just one work performed on pure aluminum (AA1100) anodized in sulphamic acid at 20°C. It showed that the higher the frequency and the higher performances in terms of hardness, thickness and compactness were achieved [31]. Such a systematic comparison is not available for alloyed aluminum instead.

Within fast-pulse philosophy, contrarily to the results of the previous study, another work on AA6061 in sulphuric-oxalic acid at 10-20°C revealed that higher frequencies increase oxide defectiveness [36].

As far as duty cycle¹ is concerned, most studies in different conditions are concordant that a DC of 70-80% brings the best oxide performances [31], [35], [36], [43]. A DC of 50% could as well be employed [33], [34] when the aim is to reduce defects in alloys particularly

¹ Duty cycle (DC) is a parameter which indicates the fraction of the period where a high current pulse is set up; $DC = t_{on} / (t_{on} + t_{off})$.

difficult to be anodized. Anyway, values higher than ~80% are too close to direct current conditions, thus annulling pulsed current benefits; values lower than ~50% give great stress to “off” pulses, increasing too much acid dissolution over oxide growth.

With respect to current “on” and “off” levels, most studies employed a range of 20-45 mA/cm² for the former and -10-10 mA/cm² for the latter [30], [31], [33], [34], [37], [38], [43]. Some studies show that a cathodic “off” current (reverse pulse) brings better results in terms of corrosion resistance, oxide hardness and rugosity when applied to AA2024-T3 anodized in sulphuric acid at 20°C and in a sulphuric-modified bath [37], [44]. Against, others authors show that, in a sulphuric-anodized 5XXX alloy, reverse pulse modality causes a greater entrapment of electrolyte anions inside the oxide and considerable hydrogen evolution phenomena that weaken the anodic oxide [39]. Gudla et al. further observed that reverse pulse modality induces, in sulphuric-anodized magnetron sputtered Al-Zr and Al-Ti, a diffused pore branching and promotes intermetallics incorporation inside the oxide [40].

In the light of this scenario, this work focused on the attempt of creating comparability conditions which could make it possible to study the influence of those electric parameters (frequency and “on”/“off” current levels) whose effect in literature is not unilateral and consolidated mostly due to data coming from different boundary conditions. For this purpose, the most largely adopted heat treatable alloys (AA2024-T3, AA6082-T6 and AA7075-T6) were hard anodized in a traditional sulphuric acid bath. The anodic depth-profile hardness, defectiveness, volumetric expansion ratio, faradic efficiency and *Voltage versus time* plot were evaluated in order to select the conditions that led to the best performances achievable.

2. MATERIAL AND METHODS

2.1 Hard anodizing tests

Hard anodizing treatment was performed in a laboratory pilot plant, schematically outlined in Figure 1 and similar to that adopted in our previous work [33]. It consists of a galvanostat/potentiostat (AMEL Instrument 2055) connected to a programmable function generator (AMEL Instrument 568) (element 1), an ammeter (Keithley 2000) (element 2), a voltmeter (element 3), a voltage divider (element 4) connected to a computer synchronized data-logger (PicoScope 2000 via software PicoLog Recorder) (elements 5 and 6) and an anodizing cell (element 7). The voltage divider is necessary in order to divide real experimental potential values (1 - 85 V) by a constant factor thus obtaining voltage data in a range suitable for the employed data logger (1 - 10 V). The supplementary battery (E_s) is added in series to the main potentiostat (E), in a secondary circuit branch activatable with a switch, in order to increase plant voltage limit value.

The cell consists of a glass container with a hollow interspace in its walls connected to a thermocryostat (Julabo F32) cooling circuit (element 8); it contains an AA 6060 bar cathode (element 9), a heat treated aluminum sample disk (14 mm of diameter and about 2 mm of thickness) as working electrode, properly placed into a holder 1 cm distant from the cathode and which allows to maintain a constant circular exposed area (1.0 cm²) (element 10), an insufflating air system for bath agitation (element 11), a thermometer and the electrolytic solution (element 12).

Bath associated variables (solution temperature, Al^{3+} and H_2SO_4 concentrations) for AA2024-T3 and AA7075-T6 had been studied in our previous works [33], [34]; best results had been obtained with $T=-2^{\circ}C$, 190 g/L H_2SO_4 and 8 g/L Al^{3+} . Preliminary tests for finding appropriate bath parameters for AA6082-T6 were carried out. With the aforementioned parameters this particular alloy showed the main issue of an exponential potential growth as process went on; it quickly reached hundreds of volts so getting to voltage plant limit value

before test end. For this reason, a higher temperature of 16°C was employed. It allowed to gain a higher acid dissolution which avoided the potential to rise up excessively, so compromising process success, but in parallel allowed to gain good oxide properties anyway.

As regards electrical cycle, the same procedures, whose settings are outlined in Table I, were performed for each alloy, AA2024-T3 (Cu 3.8-4.9%, Mg 1.2–1.8%, Mn 0.3–0.9%, Fe, Si < 0.5%, Zn < 0.25%, Ti < 0.15%, Cr < 0.1%) [45], AA6082-T6 (Si 0.7-1.3%, Mg 0.6-1.2%, Mn 0.4-1.0%, Fe < 0.5%, Cr < 0.25%, Zn < 0.2%, Cu, Ti < 0.1%) [46] and AA7075-T6 (Zn 5.1-6.1%, Mg 2.1-2.9%, Cu 1.2-2.0%, Cr 0.18-0.28%, Fe < 0.5%, Si < 0.4%, Mn < 0.3%, Ti < 0.2%) [47]. In order to ensure the best tests comparability, a common provided theoretical charge and a common duration are set between all the samples, respectively 100 C/cm² (calculated as the integral of imposed current over time and chosen in order to obtain a 50-60 µm coating, largely adopted in industrial practice) and 55 min. A duty cycle (DC) of 75% was employed since it is in the most largely adopted range in literature (70-80%) [31], [35], [36], [43]. Similarly, an average imposed current of 30 mA/cm² was employed since it is a mean value falling in the range of currents found in literature and commonly used in industrial practice (20-45 mA/cm²) [30], [31], [33], [34], [37], [38], [43]. At first, four frequencies (0.05 Hz, 0.5 Hz, 5 Hz, and 50 Hz) were tested with the same I_{on} and I_{off}, respectively 38 mA/cm² and 6 mA/cm². Then, the two frequencies which gave the best results for each alloy (in terms of oxide hardness and defectiveness) were tested with two different pulse current levels (36/12 mA/cm² and 40.5/-1.5 mA/cm²) thus studying I_{on}-I_{off} amplitude influence.

Amongst the latter tests, some with a cathodic “off” pulse are also performed. During these pulses, AA6060 cathode is subjected to an anodic current and so a little oxidation occurs. The current density and its time of application are anyway so low (1.5 mA/cm² applied for 25% of the period) that the oxide dissolution is far preponderant over its growth. Formation of an electric resistant oxide layer on the cathode is so prevented. The cathode was anyway

periodically polished with FEPA#1200 SiC emery paper in order to be sure that no surface alterations distorted the correct passage of current.

Just before each anodization, the sample disk was polished with FEPA#1200 SiC emery paper; afterwards it was cleaned with acetone and rinsed in distilled water.

2.2 Characterization techniques

Hard anodized sample coatings obtained were characterized with the following measures and parameters:

- i) linear defects density at the Alloy/Oxide interface: a qualitative parameter obtained by counting the number of defects (esteemed as critical) found at the alloy/oxide interface in the cross section observed at 200X optical microscopy (LEICA DMI5000M) magnification. The number of the defects was then assigned to 5 classes (+ : 0-3; ++ : 4-6; +++ : 7-10; ++++ : 11-15; +++++ : >15 defects/cm). Cross section was achieved embedding hard anodized sample in epoxy resin, cutting it with a Struers Labotom-3 cutting machine; the exposed cross section was then polished with emery papers and diamond suspensions (3 μm and 1 μm). Embedment was always carried out 5 days after the anodizing treatment in order to let the oxide seal naturally in atmospheric conditions;
- ii) L^* : parameter of CIELab colour space measured with a spectrophotometer (X-rite series SP60). It indicates anodic oxide lightness level; the lower is L^* value, the darker is the oxide surface. In industrial practice, darker oxides are usually related to better compactness and mechanical properties. For each sample a mean value is reported; it was obtained from seven measures acquired about 2 hours after the anodizing treatment in order to let the anodic oxide stabilize (natural sealing) in atmospheric conditions;
- iii) $HV_{0.05}$: mean value obtained from nine micro-hardness measures acquired adopting a Wolpert 402MVD micro-Vickers hardness indenter and setting 490 mN as load and 10 s as

dwel time; in particular, each sample was characterized with three profiles of three indentations performed at different oxide depths;

iv) Oxide Thickness: average of ten thickness measures acquired in different regions in the oxide cross section observed with LEICA DMI5000M optical microscope at 200X magnification;

v) V_{ox}/V_{met} : volumetric expansion ratio, an experimental parameter calculated with the same method adopted in our previous works [33], [34] and inspired by other studies [48], [49]. It is used as an index of oxide compactness and porosity. These properties can be evaluated by comparing the experimental V_{ox}/V_{met} with the theoretical Pilling-Bedworth Al/Al₂O₃ ratio (1.275): in particular, high values of this parameter suggest poor oxide density, which means a larger distribution of coating defects or porosity.

vi) η : hard anodizing faradic efficiency, estimated as [33] a ratio between the alloy effective mass converted into oxide during the process and the theoretical mass that would be ideally converted applying Faraday's Law. The equation was filled setting 100 C/cm² as total theoretical charge transferred and, as average number of electrons exchanged, average density and average molar mass, respectively 2.9511, 2.78 g/cm³ and 27.79 g/mol for AA2024-T3, 2.9553, 2.70 g/cm³ and 27.14 g/mol for AA6082-T6 and 2.9310, 2.81 g/cm³ and 28.19 g/mol for AA7075-T6.

3. RESULTS AND DISCUSSION

3.1 Frequency influence

0.05 Hz, 0.5 Hz, 5 Hz and 50 Hz were tested on the three different alloys adopting 38 mA/cm^2 as I_{on} , 6 mA/cm^2 as I_{off} , 75% as DC and 100 C/cm^2 as theoretical charge transferred (compare Table I). Looking at *Voltage versus time* plots (Figures 2,3,4), significantly different behaviors are found between different alloys; this result confirms how different precipitates and alloying compositions play a crucial influence on anodizing treatment. AA7075-T6 shows a linear potential growth not influenced by frequency (Figure 4). AA2024-T3 shows a different increasing trend (as frequency reduces, the potential tends to grow up in shorter times) (Figure 2). AA6082-T6 shows an almost constant trend for all the frequencies except for the lowest where an exponential growth occurs (Figure 3). Higher frequencies seem to destabilize barrier layer so avoiding the creation of a compact resistance to current passage. Probably at higher frequencies *off* periods are so short that prevent the complete removal of oxygen evolved in reactions occurring at Cu-rich and Fe/Mn-rich intermetallics [4], [8]; the bigger difficulty for oxygen to flow out at higher frequencies mines the compactness of barrier layer more than at lower frequencies. This hypothesis explains the behavior of AA2024-T3, where Cu-rich particles are abundant, and of AA6082-T6, whose Mn-impurity content is higher than that of AA7075-T6 [46], [47]. Moreover 6XXX series alloys are known for their easy tendency to be anodized and for producing hard and compact oxides [1] so justifying the significant growth encountered at 0.05Hz. AA7075-T6, due to its preponderance of Zn/Mg alloying content whose precipitates don't induce oxygen evolution [4], is not influenced by this hypothesized frequency-induced phenomenon. In line with these considerations, faradic efficiency (compare Table II and Figure 5) is sensibly higher at 0.05 Hz, than at higher frequencies, both for AA2024-T3 and AA6082-T6 in a more pronounced way than in AA7075-T6. Therefore at higher frequencies more parasitic phenomena are induced. As a result, in AA2024-T3 a well visible defectiveness increase is found at higher

frequencies (Table II and Figure 6); many voids (dark spots), caused by oxygen evolution reactions occurring beside Cu-based intermetallics, are in fact well spread along the oxide. Its defectiveness is anyway lower than that obtained with direct current in our previous work [33]. Contrarily, in AA6082-T6 the worst defective state is found at 0.05 Hz with a heavy jagged Al/Ox interface (Figure 6) probably due to the exponential potential rise. Indeed the latter is a variable, in addition to high amount of alloying elements and impurities, known for enhancing the genesis of anodic oxide defects [1], [33], [34]. AA6082-T6 critical issues are predominantly caused by Fe/Mn impurities; at higher frequencies they produce a sufficient amount of parasitic reactions to induce the destabilization of barrier layer and of its electric resistance. The amount of Fe/Mn is anyway not as high as the critical Cu content present in AA2024-T3, so the amount of parasitic reactions occurring in AA6082-T6 at high frequencies is not sufficient to induce the critical flaws at alloy/oxide interface found in AA2024-T3. Due to the presence of less critical issues, in AA6082-T6, a smaller porosity and voids production allows the obtainment of a denser and more compact oxide, as visible in its lower V_{ox}/V_{Al} (Figure 5). Furthermore, despite its greater compactness, it is also thicker probably due to the intrinsic volumetric expansion properties of the oxidation of its precipitates (in particular Si/SiO₂ has a high theoretical Pilling-Bedworth ratio of 1.88 which becomes even higher when amorphous and hydrated oxide, typically created by hard anodizing [1], are involved). In order to confirm this hypothesis, some EDS spectra in different region of ESEM cross section of the sample were acquired (see Figure 7 and Table III). In Figure 7 (BSD detector was used) many bright intermetallics are clearly detectable into the alloy matrix (see spectrum 1 in Table III for the typical chemical composition of these compounds) while a far lower quantity of the same bright particles is present in the anodic oxide. Hence we can assume that, while some precipitates are embedded unoxidized inside the oxide (spectrum 2), the majority of them is oxidized. In addition, spectrum 3 shows traces of Si in a region of the oxide where

no intermetallics are visible², so this silicon is probably oxidized. These experimental results suggest that Si-rich particles contribute to expand the oxide volume during the anodization of the alloy. Cu-based precipitates in AA2024-T3 moreover contribute to the creation of an instable, pore-diffused and softer oxide due to their inhomogeneous oxidation after enrichment phenomena and due to their catalytic effect on oxygen evolution reaction [8], [19], [20]. This kind of oxide is more easily dissolved by acid bath so it “looses” more coating microns at film/electrolyte interface during treatment and this justifies AA2024-T3 minor thickness. Another confirmation about more parasitic reactions occurring at higher frequencies is related to volumetric expansion ratio (compare Table II and Figure 5). It is indeed the lowest at 0.05 Hz both for AA2024-T3 and AA6082-T6 so indicating the obtainment of a more compact oxide at low frequencies; on the other hand at higher frequencies parasitic reactions produce more voids and porosity making the oxide less compact. As a result of a bigger amount of porosity and so of a less dense oxide, anodic thickness increases; in fact slight thickness increases are found as frequency rises both in AA2024-T3 and AA6082-T6 (Table II and Figure 5). Regarding AA7075-T6, as expected from its voltage plot (Figure 4), which has a frequency-independent trend, no significant variations are caused on properties analyzed. An almost constant trend is visible for thickness and V_{ox}/V_{Al} (Table II and Figure 5); the faradic efficiency is a bit higher at 0.05 Hz (same behavior seen for the other two alloys) and it is in general significantly higher than the efficiency of other tested alloys (in particular it's always upper than 95%). Therefore, although also in this case at higher frequencies more parasitic reactions occur, overall amount of them is so limited that it does not affect other properties and defective state on this alloy (compare Table II and Figures 5,6). As a result of an overall greater efficiency, also an overall higher thickness is encountered since less charge is dispersed in parasitic non-growth reactions. A curious relatively low compactness (high V_{ox}/V_{Al}) is found instead. Since less

² In order to be sure that the Si traces detected in spectrum 3 do not come from Si-based intermetallics laying under the analyzed surface, many spectra were acquired in different oxide areas where no visible intermetallics are present.

parasitic reactions, also less voids creation occur, but this is in contrast with the greater porosity indicated by the high V_{ox}/V_{Al} . The latter could therefore be ascribed to an intrinsic bigger pore morphology induced on anodic porous layer by high Zn content in the alloy. As for coating mean hardness (Table II and Figure 5), for all the alloys (with the exception of a slightly increase with the frequency for AA2024-T3) a basically constant trend is considered also taking into account their high standard deviation. The latter is for most a consequence of different values found in different test regions (Figure 8), globally greater in oxide layers nearer to Al interface and lower in layers beside external surface. Therefore anodic oxide hardness seems not to be much influenced by frequency. The greater mean values obtained in this work, compared to our previous ones [33], [34], are induced by higher mean current density which is the most hardness-influencing electric variable as already reported [50]. Anyway, constant or higher hardness at higher frequencies combined with a lower compactness is a peculiar result (usually a less compact oxide is also softer than a more compact one); maybe the amount of pores in the porous layer at higher frequencies is actually higher than at lower ones but more homogeneously distributed.

3.2 Current amplitude influence

Two additional current level combinations were tested for the two frequencies which gave the best results for each alloy (in terms of oxide hardness and defectiveness). In particular a combination with 40.5 mA/cm² as I_{on} and -1.5 mA/cm² as I_{off} (reverse pulse) and another one with 36 mA/cm² as I_{on} and 12 mA/cm² as I_{off} (compare Table I) were tested. In general, better oxide properties are found as wave amplitude ($I_{on} - I_{off}$) increases (compare Table II and Figure 9). Thickness increases are globally found when a reverse pulse modality ($I_{on} - I_{off} = 42$ mA/cm²) is adopted while it appears almost constant in the other two conditions; in addition with the increase of the wave amplitude, a significant enhancement in terms of oxide compactness is obtained. High thickness and compactness encountered with reverse modality

are explained considering cathodic current during “off” pulses; as already proven, it promotes the incorporation of intermetallics into anodic oxide [40]. It can be hypothesized that cathodic “off” current cathodically protects intermetallics more than Al matrix. Then, during “on” pulses, the intermetallics remain a bit polarized by that phenomenon occurring in “off” phases and so they remain with a tendency to be oxidized lower than the matrix. Oxidation is then shifted in the areas around intermetallics so inducing their embedment into the coating. Method adopted to calculate the V_{ox}/V_{Al} ratio [34] should be considered to understand why the embedment of intermetallics induces higher compactness. V_{ox}/V_{Al} ratio gets lower (higher compactness) as anodic growth is concentrated towards the inside of the alloy (i.e.: at the end of the process V_{ox}/V_{Al} ratio will be lower if Al/Ox interface results more distant from initial aluminum external surface), so the forced oxidation shift behind the intermetallics induced by reverse modality promotes a V_{ox}/V_{Al} decrease. Moreover cathodic current probably stimulates H^+ local reduction to H_2 , decreasing acid dissolution and consequently thickness loss during treatment. These reverse-pulse-induced phenomena (incorporation of intermetallics and H^+ local reduction to H_2) also explain the greater hardness and faradic efficiency found. For the hardness: a lower acid dissolution and the incorporation of hard intermetallics in the oxide make the coating globally slightly harder. About faradic efficiency increase, the reason is the same for the decrease of V_{ox}/V_{Al} parameter: efficiency increases as anodic growth focuses inwards. Therefore the efficiency increase does not indicate that with the same transferred charge more aluminum is converted, but it only appears in this way. It rises because the unoxidized intermetallics embedded in the oxide lead to overestimate the converted aluminum volume. Regarding AA7075-T6, also in this case a smaller dependence between oxide properties and electrical parameters is encountered: hardness is slightly higher with reverse pulse modality while faradic efficiency and V_{ox}/V_{Al} appear practically constant. Since these values are constant, maybe the incorporation of intermetallics does not take place or it takes place in a smaller amount, while hardness little increase is only due to less acid dissolution as

a consequence of H^+ reduction. Oxide color can confirm this hypothesis: this alloy does not darken with reverse pulse as the other ones do (compare L^* parameter in Table II), and usually the incorporation of intermetallics makes the oxide color darker [40]. The absence of this embedment is probably explained since Zn/Mg-based intermetallics have higher reactivity than Al matrix [4]. Therefore they do not encounter preferential cathodic protection against oxidation as previously hypothesized for the intermetallics of the other alloys. Between the two others amplitudes, 24 mA/cm^2 ($I_{\text{on}} = 36$; $I_{\text{off}} = 12$) and 32 mA/cm^2 ($I_{\text{on}} = 38$; $I_{\text{off}} = 6$), no significant changes appear. A slightly lower hardness results in the latter probably due to really low “off” current; it has indeed an easier tendency to distribute itself inhomogenously around intermetallics so creating anodic inner tensions. Concerning defectiveness, as shown in Table II, wave amplitudes do not affect it within the range analyzed. It is curious how side reactions occurring during cathodic “off” pulses do not enhance the oxide defective state; probably cathodic current is so low (-1.5 mA/cm^2) that side reactions, as gaseous hydrogen evolution, are so limited that do not create particular critical issues.

4. CONCLUSIONS

AA2024-T3, AA6082-T6 and AA7075-T6 have been hard anodized in a traditional sulphuric acid bath with different pulsed current frequencies and current amplitudes; the most important conclusions which can be drawn are:

- i. the different alloys show very different behaviors, confirming how different precipitates and alloying compositions play a crucial influence on anodizing treatment;
- ii. an increase of the pulsed current frequency induces a reduction of the coating electric resistance (probably due to a barrier layer destabilization). For this reason, this strategy could be exploited for energy saving issues or to avoid steep voltage growths which are critical for defects genesis as encountered in AA6082-T6;
- iii. an increase of the pulsed current frequency induces a greater difficulty to overcome critical issues caused by intermetallics (inhomogeneities during growth and parasitic reactions as oxygen evolution). In these conditions critical alloys, such as high Cu-content AA2024-T3, lead to a harder coating but much more flawed. Where the content of critical elements is lower but not negligible, such as in AA6082-T6, no more defects occur at high frequencies, anyway a less compact and so slightly thicker oxide results. In the alloys characterized by intermetallics which do not induce critical oxygen evolution reactions, such as in AA7075-T6 with Zn and Mg as main alloying elements, the frequency effect is basically negligible;
- iv. reverse pulse modality allows to obtain a thicker and harder oxide thanks to a lower local acid dissolution caused by hydrogen reduction during “off” periods; despite this gas generation, the employment of a really low cathodic current (-1.5 mA/cm^2) does not provoke an increase of the oxide defectiveness. Moreover in AA2024-T3 and AA6082-T6, reverse pulse promotes the incorporation of intermetallics into the anodic coating leading to greater oxide hardness and compactness;

- v. too low “off” current values (but still anodic) lead to a slight hardness decrease, due to an easier tendency of the current to distribute inhomogeneously around intermetallics so creating anodic inner tensions;
- vi. within wave amplitudes tested, no significant variations in defective state are encountered.

5. REFERENCES

- [1] P. G. Sheasby and R. Pinner, *The Surface Treatment and Finishing of Aluminum and Its Alloys*, 2 Vol, 6th ed. ASM international, pp 743-811, 2001.
- [2] A. K. Vasudevan and R. D. Doherty, *Aluminum Alloys - Contemporary research and applications*, Vol 31. Academic Press Inc., 1989.
- [3] S. C. Wang and M. J. Starink, "Precipitates and intermetallic phases in precipitation hardening Al-Cu-Mg-(Li) based alloys," *Int. Mater. Rev.*, vol. 50, no. 4, pp. 193-215, 2005.
- [4] M. Saenz de Miera, M. Curioni, P. Skeldon, and G. E. Thompson, "The behaviour of second phase particles during anodizing of aluminium alloys," *Corros. Sci.*, vol. 52, no. 7, pp. 2489-2497, 2010.
- [5] A. K. Mukhopadhyay, "On the Nature of the Fe-Bearing Particles Influencing Hard Anodizing Behavior of AA 7075 Extrusion Products," *Surf. Coatings Technol.*, vol. 92, no. 3, pp. 212-220, 1997.
- [6] A. K. Mukhopadhyay, V. V. Rama Rao, and C. R. Chakravorty, "The influence of constituent particles on the quality of hard anodic coatings on fully heat treated AA 7075 extrusion products," *Mater. Sci. Forum*, vol. 217-222, no. PART 3, pp. 1617-1622, 1996.
- [7] L. E. Fratila-Apachitei, J. Duszczyk, and L. Katgerman, "Voltage transients and morphology of AlSi(Cu) anodic oxide layers formed in H₂SO₄ at low temperature," *Surf. Coatings Technol.*, vol. 157, no. 1, pp. 80-94, 2002.
- [8] M. Saenz de Miera, M. Curioni, P. Skeldon, and G. E. Thompson, "Preferential anodic oxidation of second-phase constituents during anodising of AA2024-T3 and AA7075-T6 alloys," *Surf. Interface Anal.*, vol. 42, no. 4, pp. 241-246, Apr. 2010.
- [9] R. D. Guminski, P. G. Sheasby, and H. J. Lamb, "Reaction rates of second-phase constituents in aluminium during etching, brightening and oxalic acid anodizing processes," *Trans. Inst. Met. Finish.*, no. 46, pp. 44-48, 1968.
- [10] J. Cote, E. E. Howlett, and H. J. Lamb, "Behavior of intermetallic compounds in aluminium during sulfuric acid anodizing," *Plating*, no. 57, pp. 484-496, 1970.
- [11] M. Saenz de Miera, M. Curioni, P. Skeldon, and G. E. Thompson, "Modelling the anodizing behaviour of aluminium alloys in sulphuric acid through alloy analogues," *Corros. Sci.*, vol. 50, no. 12, pp. 3410-3415, 2008.
- [12] M. Curioni, M. Saenz de Miera, P. Skeldon, G. E. Thompson, and J. Ferguson, "Macroscopic and Local Filming Behavior of AA2024 T3 Aluminum Alloy during Anodizing in Sulfuric Acid Electrolyte," *J. Electrochem. Soc.*, vol. 155, no. 8, p. C387, 2008.
- [13] A. K. Mukhopadhyay and A. K. Sharma, "Influence of Fe-bearing particles and nature of electrolyte on the hard anodizing behaviour of AA 7075 extrusion products," *Surf. Coatings Technol.*, vol. 92, no. 3, pp. 212-220, 1997.
- [14] L. E. Fratila-Apachitei, H. Terryn, P. Skeldon, G. E. Thompson, J. Duszczyk, and L. Katgerman, "Influence of substrate microstructure on the growth of anodic oxide layers," *Electrochim. Acta*, vol. 49, no. 7, pp. 1127-1140, 2004.

- [15] M. Aggerbeck, A. Junker-holst, D. V. Nielsen, V. C. Gudla, and R. Ambat, "Anodisation of sputter deposited aluminium – titanium coatings : Effect of microstructure on optical characteristics," *Surf. Coat. Technol.*, vol. 254, pp. 138–144, 2014.
- [16] V. Chakravarthy, S. Canulescu, R. Shabadi, K. Rechendorff, K. Dirscherl, and R. Ambat, "Structure of anodized Al – Zr sputter deposited coatings and effect on optical appearance," *Appl. Surf. Sci.*, vol. 317, pp. 1113–1124, 2014.
- [17] M. Jariyaboon, P. Moller, R. E. D. Borkowski, and R. Ambat, "FIB-SEM investigation of trapped intermetallic particles in anodic oxide films on AA1050 aluminium FIB-SEM investigation of trapped intermetallic particles in anodic oxide films on AA1050 aluminium," *Anti-Corrosion Methods Mater.*, vol. 58, no. 4, pp. 173–178, 2011.
- [18] K. Shimizu, G. M. Brown, K. Kobayashi, P. Skeldon, G. E. Thompson, and G. C. Wood, "Ultramicrotomy a route towards the enhanced understanding of the corrosion and filming behaviour of aluminium and its alloys," *Corros. Sci.*, vol. 40, pp. 1049–1072, 1998.
- [19] L. Iglesias-Rubianes, S. J. Garcia-Vergara, P. Skeldon, G. E. Thompson, J. Ferguson, and M. Beneke, "Cyclic oxidation processes during anodizing of Al–Cu alloys," *Electrochim. Acta*, vol. 52, no. 24, pp. 7148–7157, Aug. 2007.
- [20] X. Zhou, G. E. Thompson, H. Habazaki, K. Shimizu, P. Skeldon, and G. C. Wood, "Copper enrichment in Al–Cu alloys due to electropolishing and anodic oxidation," *Thin Solid Films*, vol. 293, no. 1–2, pp. 327–332, Jan. 1997.
- [21] A. A. D. Sarhan, E. Zalnezhad, and M. Hamdi, "The influence of higher surface hardness on fretting fatigue life of hard anodized aerospace AL7075-T6 alloy," *Mater. Sci. Eng. A*, vol. 560, pp. 377–387, Jan. 2013.
- [22] E. Cirik and K. Genel, "Effect of anodic oxidation on fatigue performance of 7075-T6 alloy," *Surf. Coatings Technol.*, vol. 202, no. 21, pp. 5190–5201, Jul. 2008.
- [23] C. Fares, L. Hemmouche, M. A. Belouchrani, A. Amrouche, D. Chicot, and E. S. Puchi-Cabrera, "Coupled effects of substrate microstructure and sulphuric acid anodizing on fatigue life of a 2017A aluminum alloy," *Mater. Des.*, vol. 86, pp. 723–734, 2015.
- [24] B. Rajasekaran, S. Ganesh Sundara Raman, L. Rama Krishna, S. V. Joshi, and G. Sundararajan, "Influence of microarc oxidation and hard anodizing on plain fatigue and fretting fatigue behaviour of Al–Mg–Si alloy," *Surf. Coatings Technol.*, vol. 202, no. 8, pp. 1462–1469, Jan. 2008.
- [25] G. E. Thompson, L. Zhang, C. J. E. Smith, and P. Skeldon, "Boric/sulfuric acid anodizing of aluminum alloys 2024 and 7075: Film growth and corrosion resistance," *Corrosion*, vol. 55, no. 11, pp. 1052–1061, 1999.
- [26] Y. Sepulveda, M. A. Paez, J. H. Zagal, J. Henriquez, J. Pavez, A. Monsalve, O. Bustos, and G. E. Thompsons, "Anodizing of Al 2024-T3 in mixtures of sulphuric-boric acids," *Bol. la Soc. Chil. Quim.*, vol. 46, no. 4, pp. 399–407, 2001.
- [27] V. R. Capelossi, M. Poelman, I. Recloux, R. P. B. Hernandez, H. G. de Melo, and M. G. Olivier, "Corrosion protection of clad 2024 aluminum alloy anodized in tartaric-sulfuric acid bath and protected with hybrid sol–gel coating," *Electrochim. Acta*, vol. 124, pp. 69–79, Apr. 2014.

- [28] V. Raj, M. P. Rajaram, G. Balasubramanian, S. Vincent, and D. Kanagaraj, "Pulse anodizing - An overview," *Transactions of the Institute of Metal Finishing*, vol. 81, no. 4, pp. 114–121, 2003.
- [29] K. Yokoyama, H. Konno, H. Takahashi, and M. Nagayama, "Advantages of Pulse Anodizing," in *Plating and Surface Finishing*, 1982, vol. 69, no. 7, pp. 62–65.
- [30] A. D. Juhl, "Why it makes sense to upgrade to pulse anodizing," *Met. Finish.*, vol. 107, no. 7–8, pp. 24–27, 2009.
- [31] D. Kanagaraj, V. Raj, S. Vincent, and S. Venkatakrishna Iyer, "Effect of pulse frequency on pulse anodising of AA 1100 aluminium alloy in sulphamic acid," *Bull. Electrochem.*, vol. 17, no. 11, pp. 523–526.
- [32] L. . Fratila-Apachitei, J. Duszczek, and L. Katgerman, "AlSi(Cu) anodic oxide layers formed in H₂SO₄ at low temperature using different current waveforms," *Surf. Coatings Technol.*, vol. 165, no. 3, pp. 232–240, 2003.
- [33] M. Bononi, R. Giovanardi, A. Bozza, and P. Mattioli, "Pulsed current effect on hard anodizing process of 2024-T3 aluminium alloy," *Surf. Coatings Technol.*, vol. 289, pp. 110–117, 2016.
- [34] A. Bozza, R. Giovanardi, T. Manfredini, and P. Mattioli, "Pulsed current effect on hard anodizing process of 7075-T6 aluminium alloy," *Surf. Coatings Technol.*, vol. 270, pp. 139–144, 2015.
- [35] H. H. Shih and S. L. Tzou, "Study of anodic oxidation of aluminum in mixed acid using a pulsed current," *Surf. Coatings Technol.*, vol. 124, no. 2–3, pp. 278–285, 2000.
- [36] A. Rajendra, B. J. Parmar, A. K. Sharma, H. Bhojraj, M. M. Nayak, and K. Rajanna, "Hard anodisation of aluminium and its application to sensorics," *Surf. Eng.*, vol. 21, no. 3, pp. 193–197, 2005.
- [37] W. Aperador, A. Delgado, and J. Bautista, "Improved corrosion protection properties in anodic films type porous on 2024 T3 aluminium alloys obtained by pulse reverse plating," *Int. J. Electrochem. Sci.*, vol. 8, no. 7, pp. 9607–9617, 2013.
- [38] J. gang Qian, C. Wang, D. Li, B. lan Guo, and G. ling Song, "Formation mechanism of pulse current anodized film on AZ91D Mg alloy," *Trans. Nonferrous Met. Soc. China (English Ed.)*, vol. 18, no. 1, pp. 19–23, 2008.
- [39] V. C. Gudla, F. Jensen, K. Bordo, A. Simar, and R. Ambat, "Effect of High Frequency Pulsing on the Interfacial Structure of Anodized Aluminium-TiO₂," *J. Electrochem. Soc.*, vol. 162, no. 7, pp. C303–C310, 2015.
- [40] V. C. Gudla, K. Bordo, S. Engberg, K. Rechendorff, and R. Ambat, "High frequency pulse anodising of magnetron sputtered Al-Zr and Al-Ti Coatings," *Mater. Des.*, vol. 95, pp. 340–347, 2016.
- [41] V. C. Gudla, K. Bordo, F. Jensen, S. Canulescu, S. Yuksel, A. Simar, and R. Ambat, "High frequency anodising of aluminium–TiO₂ surface composites: Anodising behaviour and optical appearance," *Surf. Coatings Technol.*, vol. 277, pp. 67–73, Sep. 2015.
- [42] W. Lee, K. Schwirn, M. Steinhart, E. Pippel, R. Scholz, and U. Gösele, "Structural engineering of nanoporous anodic aluminium oxide by pulse anodization of

- aluminium.” *Nat. Nanotechnol.*, vol. 3, no. 4, pp. 234–239, 2008.
- [43] D. Kanagaraj, V. Raj, S. Vincent, B. P. Kumar, A. S. Kumar, and S. V Iyer, “Pulse anodizing of AA1100 aluminium alloy in oxalic acid electrolyte,” *Bull. Electrochem.*, vol. 17, no. Part 6. pp. 285–288, 2001.
- [44] S. Chen, C. Kang, J. Wang, C. Liu, and K. Sun, “Synthesis of anodizing composite films containing superfine Al₂O₃ and PTFE particles on Al alloys,” *Appl. Surf. Sci.*, vol. 256, no. 22, pp. 6518–6525, 2010.
- [45] “Matweb: Online Materials Information Resource; AA2024-T3.” [Online]. Available: <http://www.matweb.com/search/DataSheet.aspx?MatGUID=57483b4d782940faaf12964a1821fb61&ckck=1>. [Accessed: 01-Jun-2016].
- [46] “MatWeb: Online Materials Information Resource; AA6082-T6.” [Online]. Available: <http://www.matweb.com/search/datasheet.aspx?matguid=fad29be6e64d4e95a241690f1f6e1eb7&ckck=1>. [Accessed: 01-Jun-2016].
- [47] “MatWeb: Online Materials Information Resource; AA7075-T6.” [Online]. Available: <http://www.matweb.com/search/DataSheet.aspx?MatGUID=4f19a42be94546b686bbf43f79c51b7d>. [Accessed: 01-Jun-2016].
- [48] L. Arurault, “Pilling–Bedworth ratio of thick anodic aluminium porous films prepared at high voltages in H₂SO₄ based electrolyte,” *Trans. Inst. Met. Finish.*, vol. 86, no. 1, pp. 51–54, 2008.
- [49] G. E. J. Poinern, N. Ali, and D. Fawcett, “Progress in Nano-Engineered Anodic Aluminum Oxide Membrane Development,” *Materials (Basel)*, vol. 4, no. 12, pp. 487–526, Feb. 2011.
- [50] I. Mohammadi and A. Afshar, “Modification of nanostructured anodized aluminum coatings by pulse current mode,” *Surf. Coatings Technol.*, vol. 278, pp. 48–55, 2015.

Table I: Parameters adopted for anodizing tests performed in laboratory pilot plant.

Alloy	Sample	Bath Conditions	Electrical Parameters							
		T ; Al ³⁺ ; H ₂ SO ₄ [°C ; g/L ; g/L]	Frequency [Hz]	(I _{on} ; t _{on}) [mA/cm ² ; s]	(I _{off} ; t _{off}) [mA/cm ² ; s]	No. of pulses	Duty cycle	Charge [C/cm ²]	I _{mean} [mA/cm ²]	Duration [min]
AA2024-T3	1	-2 ; 8 ; 190	0.05	(40.5; 15)	(-1.5; 5)	166	75%	100	30	55
	2			(38; 15)	(6; 5)					
	3			(36; 15)	(12; 5)					
	4		0.5	(38; 1.5)	(6; 0.5)	1666				
	5			(38; 0.15)	(6; 0.005)	16666				
	6		50	(40.5; 0.015)	(-1.5; 0.005)	166666				
	7			(38; 0.015)	(6; 0.005)					
	8			(36; 0.015)	(12; 0.005)					
AA6082-T6	9	16 ; 8 ; 190	0.05	(38; 15)	(6; 5)	166				
	10		0.5	(40.5; 1.5)	(-1.5; 0.5)	1666				
	11			(38; 1.5)	(6; 0.5)					
	12			(36; 1.5)	(12; 0.5)					
	13		5	(38; 0.15)	(6; 0.005)	16666				
	14		50	(40.5; 0.015)	(-1.5; 0.005)	166666				
	15			(38; 0.015)	(6; 0.005)					
	16			(36; 0.015)	(12; 0.005)					
AA7075-T6	17	-2 ; 8 ; 190	0.05	(40.5; 15)	(-1.5; 5)	166				
	18			(38; 15)	(6; 5)					
	19			(36; 15)	(12; 5)					
	20		0.5	(38; 1.5)	(6; 0.5)	1666				
	21			(38; 0.15)	(6; 0.005)	16666				
	22		50	(40.5; 0.015)	(-1.5; 0.005)	166666				
	23			(38; 0.015)	(6; 0.005)					
	24			(36; 0.015)	(12; 0.005)					

Table II: Results obtained by hard anodized samples characterizations; regarding “Linear defects density at Al/Ox interface”, No. of defects per linear cm is divided into 5 classes (+ : 0-3; ++ : 4-6; +++ : 7-10; ++++ : 11-15; +++++ : >15 defects/cm).

Alloy	Sample	Linear defects density at Al/Ox interface	L*	a ; b (± 0.2)	HV _{0,05}	Oxide thickness [μm]	V _{ox} /V _{met}	η
AA2024-T3	1	+++	31.5 ± 0.1	-0.6 ; -0.7	394 ± 23	62 ± 1	1.63 ± 0.01	~100%
	2	++	35.3 ± 1.2	-1.1 ; -2.3	330 ± 26	54 ± 1	1.66 ± 0.03	90%
	3	++	34.4 ± 0.1	-1.9; -2.3	373 ± 27	55 ± 1	1.68 ± 0.01	91%
	4	+++++	33.0 ± 0.3	-0.5 ; -1.3	358 ± 30	56 ± 1	1.80 ± 0.04	87%
	5	+++++	33.2 ± 0.9	-0.3 ; -0.9	363 ± 32	56 ± 1	1.79 ± 0.02	87%
	6	++++	31.5 ± 0.1	-0.3 ; -0.9	398 ± 17	59 ± 1	1.74 ± 0.01	90%
	7	+++++	33.6 ± 0.3	-0.3 ; -0.7	370 ± 25	57 ± 2	1.79 ± 0.02	87%
	8	+++++	30.9 ± 0.1	-0.5 ; -0.9	376 ± 37	57 ± 1	1.79 ± 0.02	88%
AA6082-T6	9	++++	34.9 ± 0.2	-0.8 ; 0.0	519 ± 51	58 ± 1	1.61 ± 0.04	91%
	10	+	35.1 ± 0.2	0.6 ; 0.7	565 ± 35	63 ± 1	1.64 ± 0.01	96%
	11	+	32.2 ± 0.1	0.4 ; 0.9	526 ± 49	59 ± 1	1.69 ± 0.03	84%
	12	+	35.9 ± 0.2	0.7 ; 0.5	540 ± 39	58 ± 1	1.69 ± 0.02	87%
	13	++	36.1 ± 0.3	0.3 ; 1.1	511 ± 25	60 ± 2	1.71 ± 0.05	87%
	14	+	31.2 ± 0.1	0.5 ; 0.8	578 ± 29	61 ± 1	1.68 ± 0.02	89%
	15	+	37.5 ± 0.3	0.7 ; 2.1	521 ± 40	60 ± 2	1.72 ± 0.02	85%
	16	+	36.7 ± 0.3	0.5 ; 1.8	555 ± 31	59 ± 1	1.73 ± 0.02	88%
AA7075-T6	17	++	36.6 ± 0.0	2.0 ; 3.6	445 ± 28	65 ± 1	1.77 ± 0.01	96%
	18	++	35.5 ± 0.6	1.5 ; 2.6	419 ± 17	64 ± 1	1.78 ± 0.02	97%
	19	+++	35.6 ± 0.0	1.6 ; 3.7	433 ± 32	63 ± 1	1.79 ± 0.01	97%
	20	+++	35.4 ± 0.2	1.4 ; 3.7	407 ± 25	65 ± 1	1.78 ± 0.02	96%
	21	+++	34.8 ± 0.3	1.7 ; 2	423 ± 22	65 ± 1	1.80 ± 0.01	94%
	22	++	35.1 ± 0.1	1.8 ; 3.0	432 ± 31	68 ± 1	1.78 ± 0.02	95%
	23	++	34.5 ± 0.3	1.6 ; 2.6	410 ± 33	65 ± 1	1.78 ± 0.02	96%
	24	+++	35.1 ± 0.3	1.1 ; 2.1	418 ± 35	65 ± 1	1.79 ± 0.02	96%

Table III: Chemical compositions obtained with EDS (Energy Dispersive X-Rays Spectroscopy, *Oxford Instruments INCA300*) analyses in three different areas of sample 13 (AA6082-T6) visible in Figure 7. Spectrum1 is a spot acquisition beside an intermetallic dispersed in alloy matrix; Spectrum2 is a spot acquisition beside a non-oxidized intermetallic dispersed in anodic oxide; Spectrum3 is an area acquisition of an oxide zone where no unoxidized intermetallics are visible.

Element	Atomic%		
	Spectrum1	Spectrum2	Spectrum3
Al	83.6	55.6	35.0
Si	6.7	7.9	0.5
Mn	4.2	5.4	not detected
Fe	4.1	6.4	not detected
Mg	0.6	0.3	not detected
Cr	0.7	1.0	not detected
O	not detected	22.9	60.0
S	not detected	0.5	4.6

Figure Captions

Figure 1: Laboratory anodizing system: 1) galvanostat equipped with programmable function generator and a supplementary battery (E_s), 2) ammeter, 3) voltmeter, 4) voltage divider, 5) data logger, 6) computer, 7) electrochemical cell, 8) cooling system, 9) cathode, 10) working electrode, 11) air-agitation system, 12) electrolytic solution.

Figure 2: Voltage versus time plots registered during anodizing treatment performed at different frequencies on AA2024-T3 applying 38 mA/cm^2 as I_{on} and 6 mA/cm^2 as I_{off} . The oscillatory behaviour visible in the different plots is not the realistic one (related to the frequency applied) since data have been filtered for readability purposes.

Figure 3: Voltage versus time plots registered during anodizing treatment performed at different frequencies on AA6082-T6 applying 38 mA/cm^2 as I_{on} and 6 mA/cm^2 as I_{off} . The oscillatory behaviour visible in the different plots is not the realistic one (related to the frequency applied) since data have been filtered for readability purposes.

Figure 4: Voltage versus time plots registered during anodizing treatment performed at different frequencies on AA7075-T6 applying 38 mA/cm^2 as I_{on} and 6 mA/cm^2 as I_{off} . The oscillatory behaviour visible in the different plots is not the realistic one (related to the frequency applied) since data have been filtered for readability purposes.

Figure 5: Effect of pulsed current frequency on anodic oxide thickness, volumetric expansion ratio ($V_{\text{ox}}/V_{\text{Al}}$), mean hardness ($\text{HV}_{0.05}$) and faradic efficiency.

Figure 6: Cross section micrographs showing representative areas of coating and alloy/oxide interface morphologies in AA2024-T3, AA6082-T6 and AA7075-T6 samples anodized at different frequency values. Significant critical defects are indicated by black bold arrows; minor defects are indicated by black dashed ones.

Figure 7: ESEM (Environmental Scanning Electron Microscope, *Philips XL40*) image acquisition of sample 13 cross section (AA6082-T6) showing the zones where EDS analyses were carried out.

Figure 8: Effect on the oxide hardness depth profile ($\text{HV}_{0.05}$) of pulsed current frequency (a) and current wave amplitude ($I_{\text{on}}-I_{\text{off}}$) (b).

Figure 9: Effect of pulsed current wave amplitude ($I_{\text{on}}-I_{\text{off}}$) on anodic oxide thickness, volumetric expansion ratio ($V_{\text{ox}}/V_{\text{Al}}$), mean hardness ($\text{HV}_{0.05}$) and faradic efficiency.

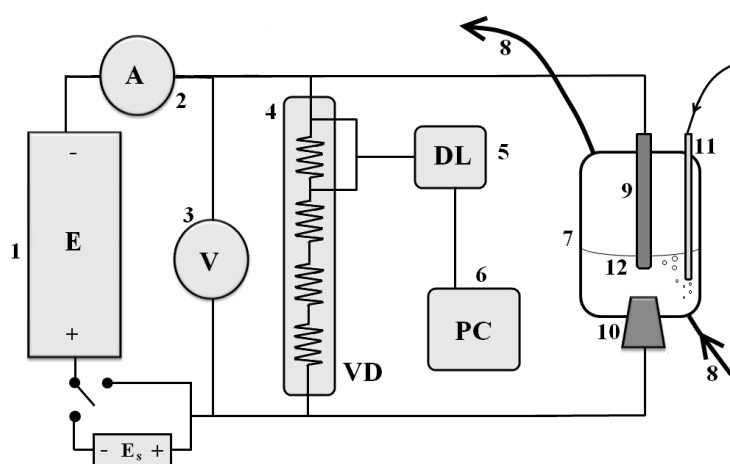


Figure 1

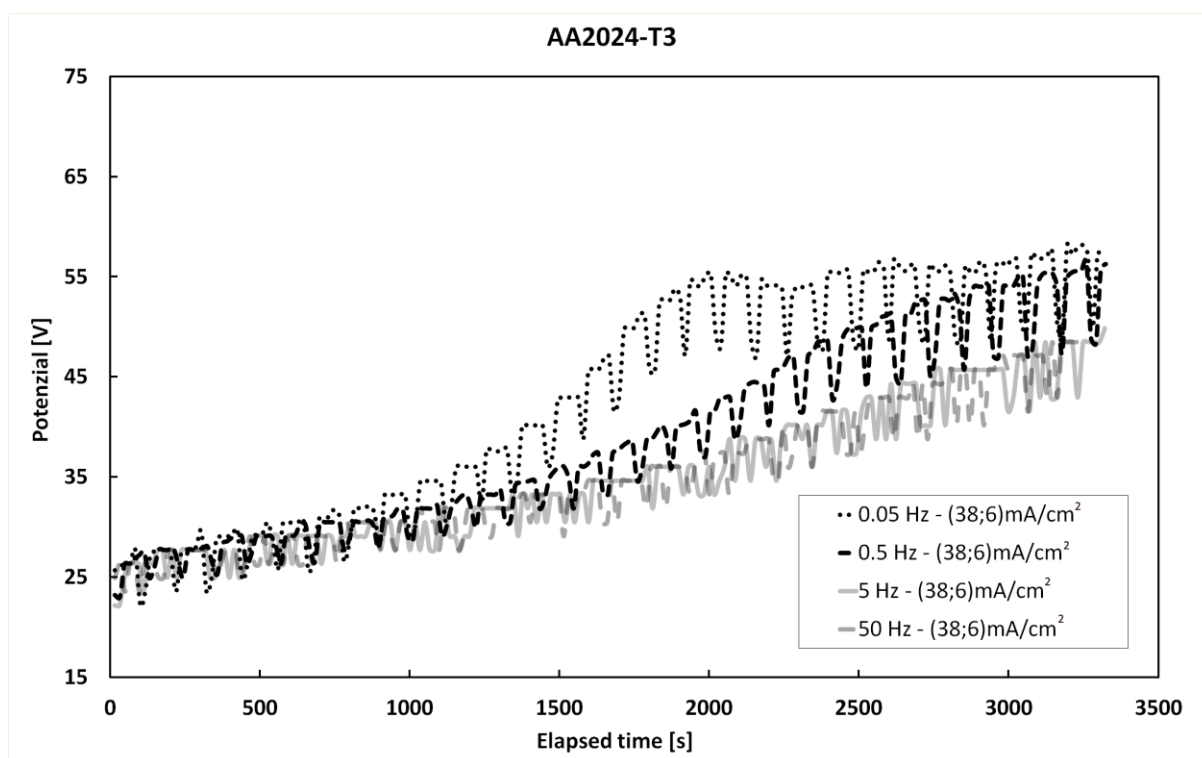


Figure 2

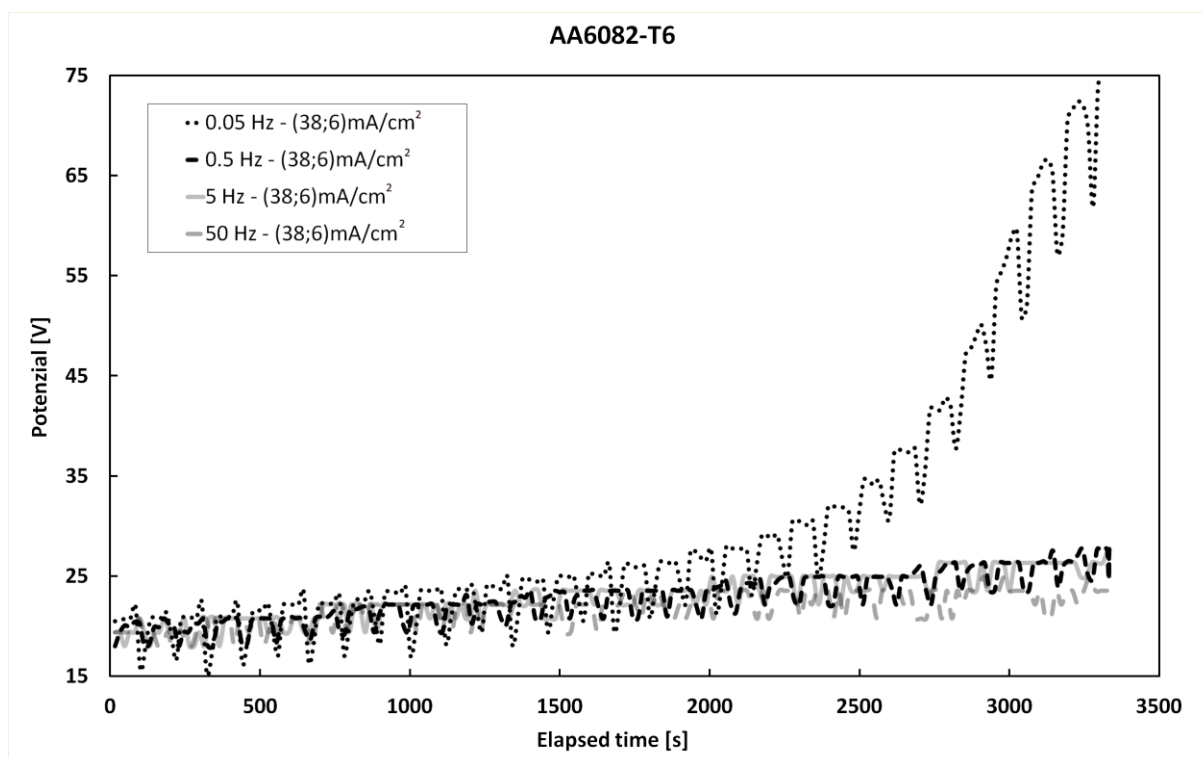


Figure 3

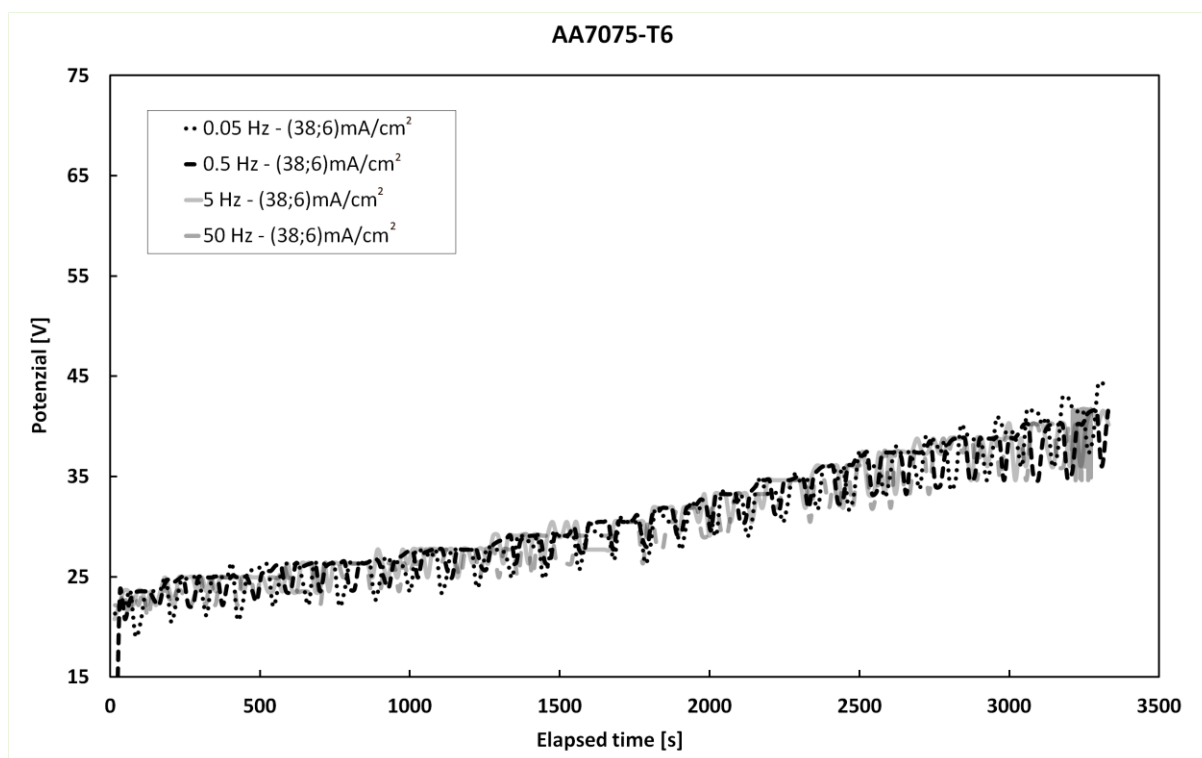


Figure 4

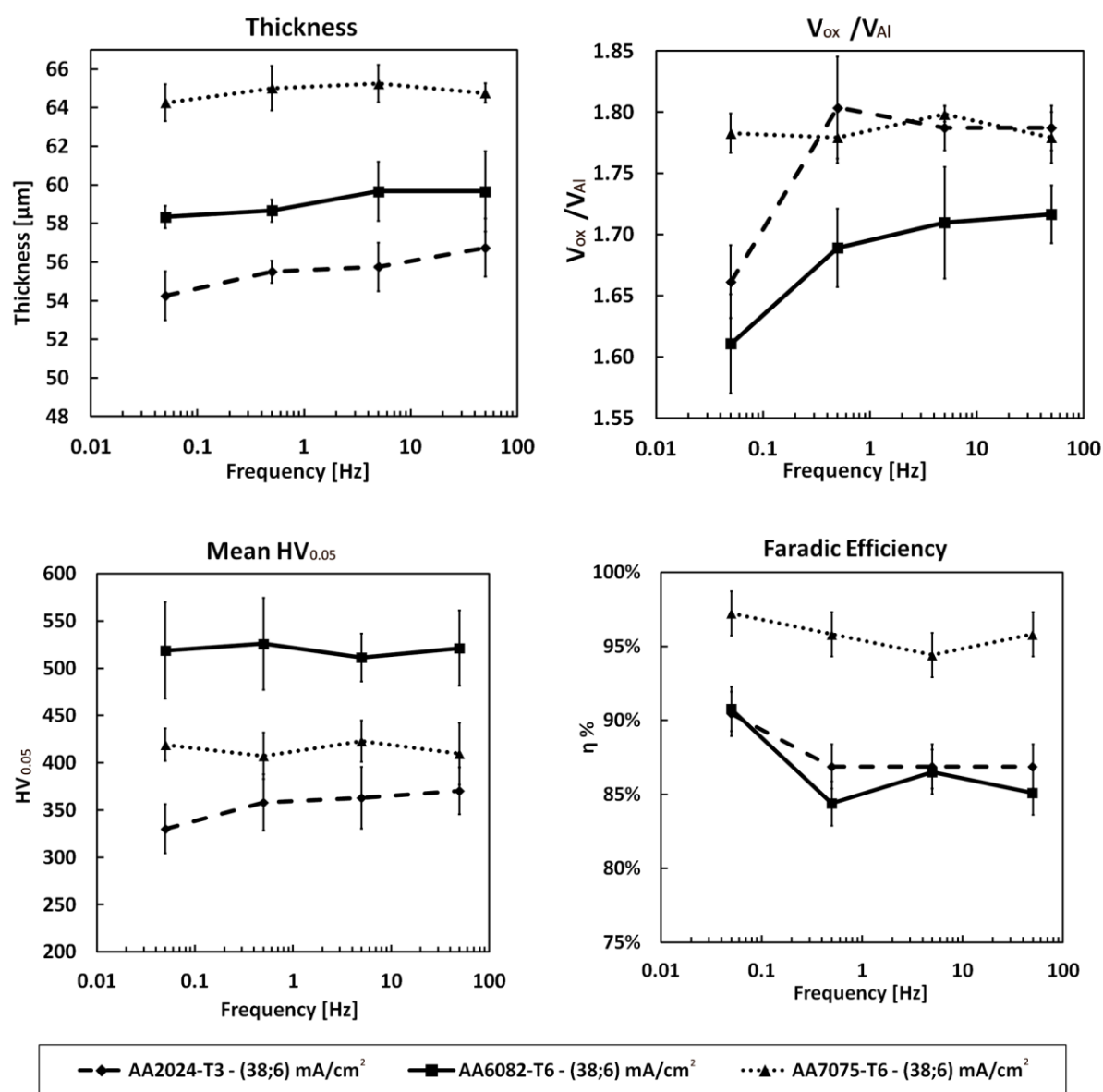


Figure 5

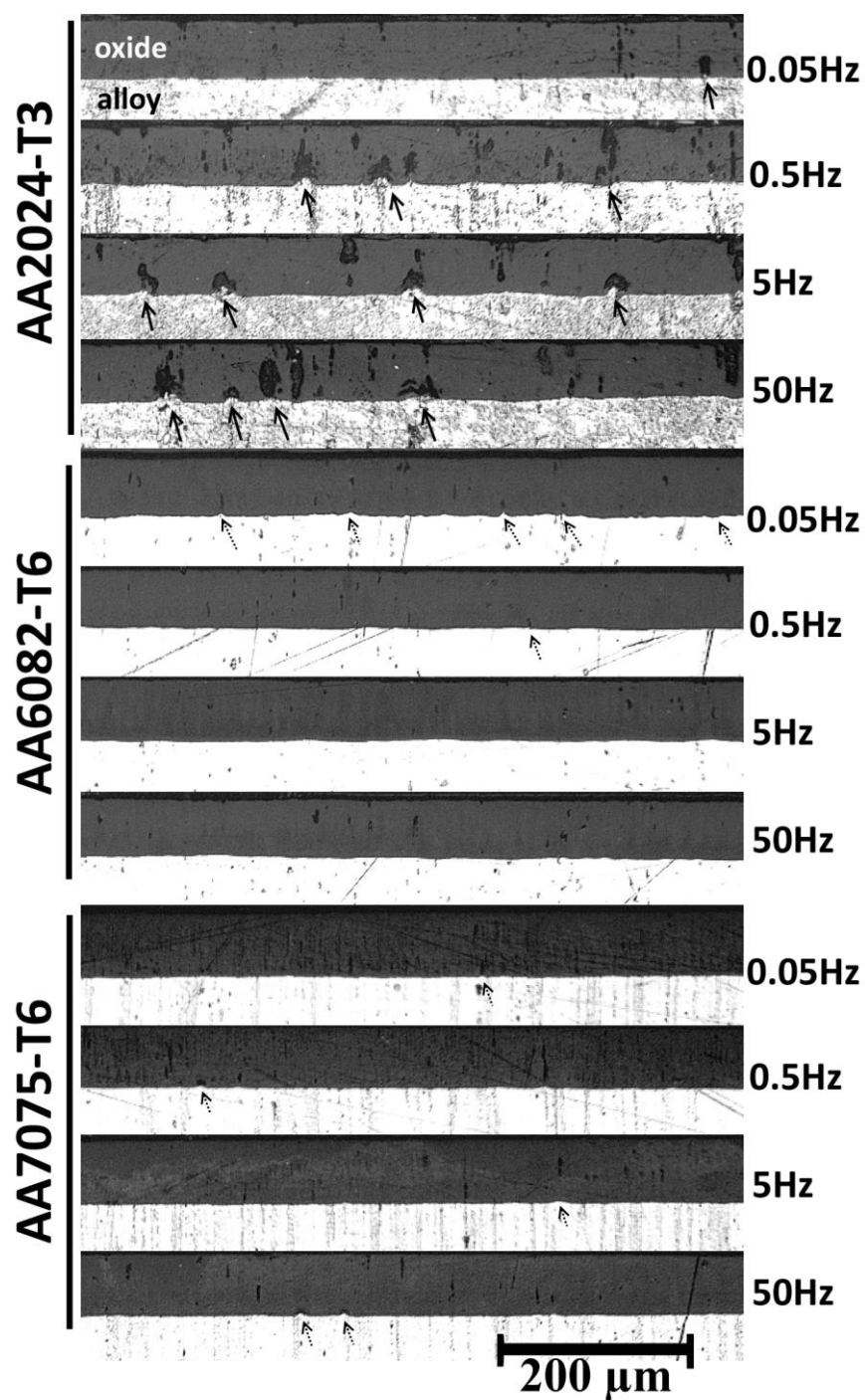


Figure 6

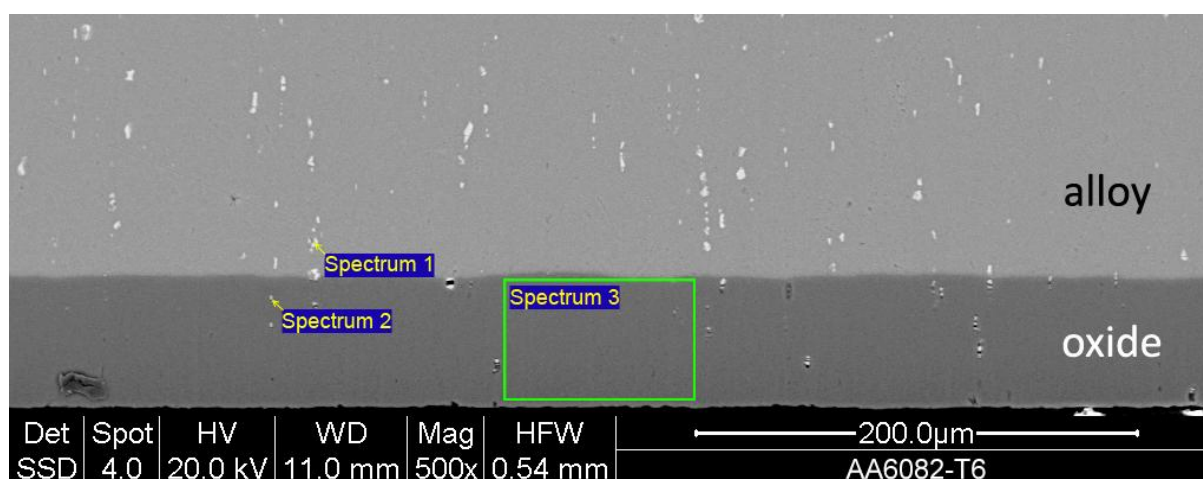


Figure 7

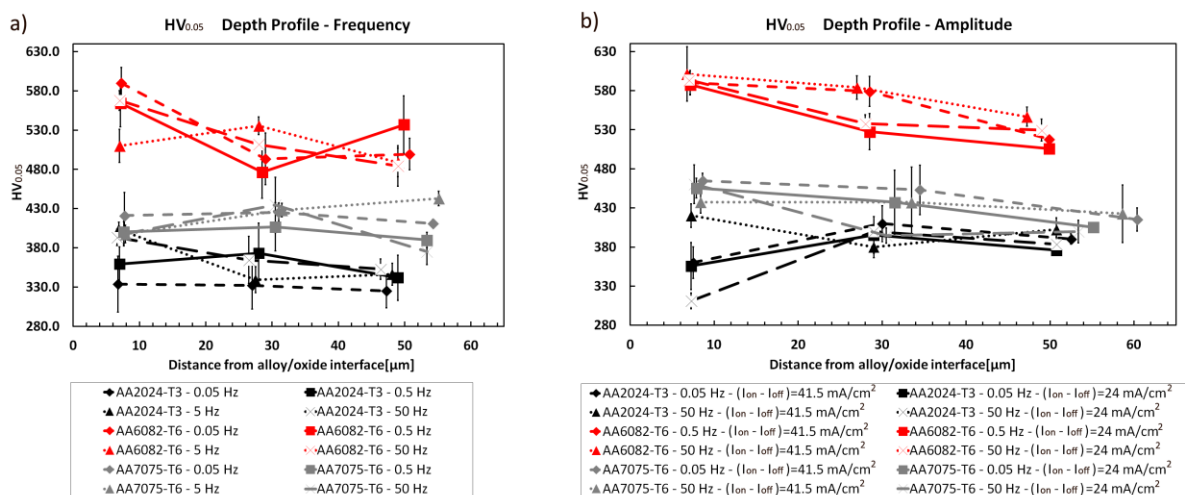


Figure 8

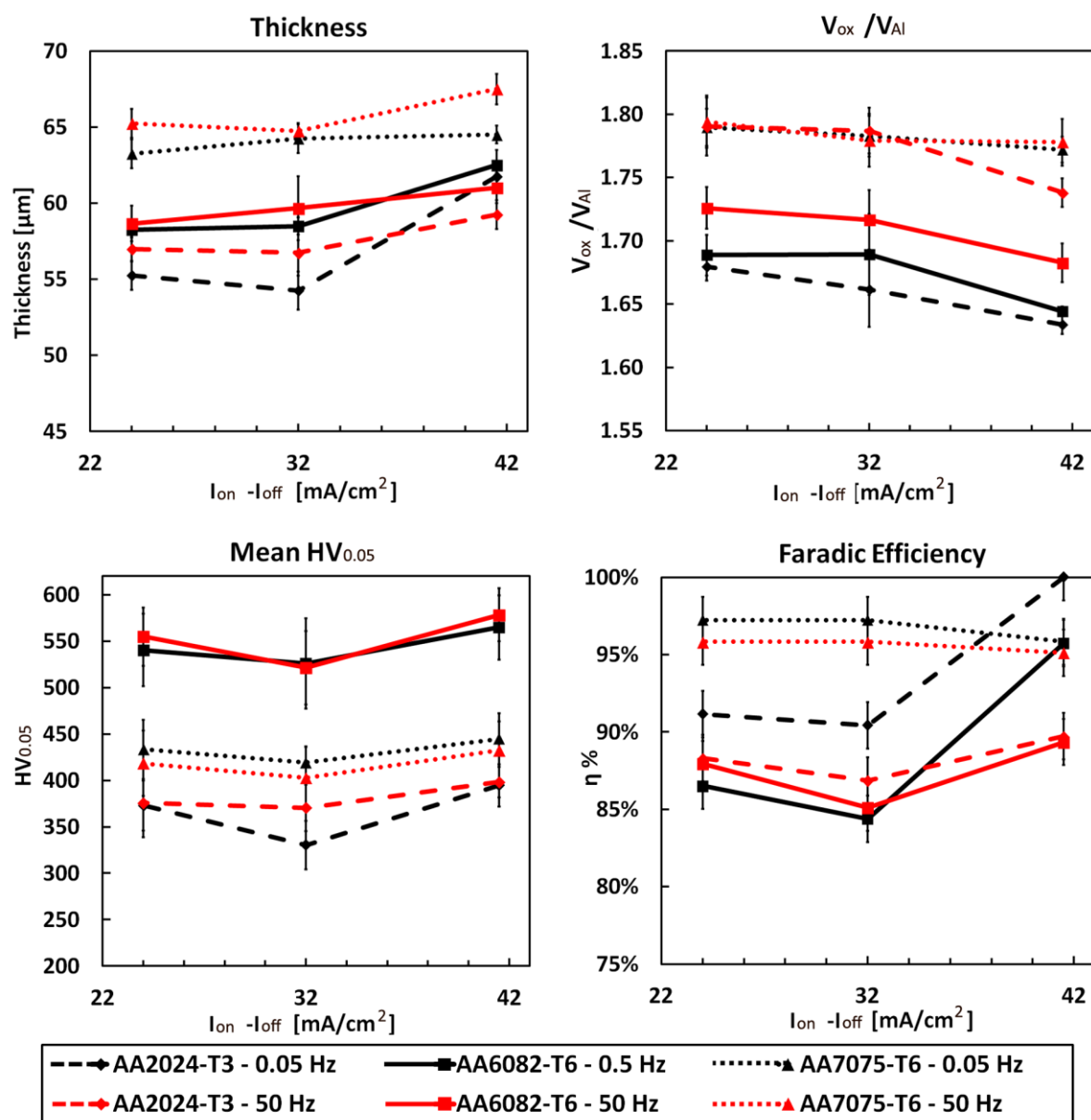


Figure 9

Highlights

- High frequencies induced coating electric resistance reduction
- High frequencies showed critical issues in improving oxide defectiveness
- Reverse pulse modality improved oxide thickness and hardness
- Low “off” anodic current led to slight hardness decrease